Stem Cell Reports
Article

ISSCR

OPEN ACCESS

Cardiac differentiation roadmap for analysis of plasticity and balanced lineage commitment

Rebecca R. Snabel,[1,4] Carla Cofiño-Fabrés,[2,4] Marijke Baltissen,[3] Verena Schwach,[2] Robert Passier,[2,5,*] and Gert Jan C. Veenstra[1,5,6,*]

[1]Department of Molecular Developmental Biology, Radboud Institute for Molecular Life Sciences, Faculty of Science, Radboud University, Nijmegen, the Netherlands
[2]Department of Bioengineering Technologies, Applied Stem Cell Technologies Group, TechMed Centre, University of Twente, Enschede, the Netherlands
[3]Department of Molecular Biology, Radboud Institute for Molecular Life Sciences, Faculty of Science, Oncode Institute, Radboud University, Nijmegen, the Netherlands
[4]These authors contributed equally
[5]Senior author
[6]Lead contact
*Correspondence: robert.passier@utwente.nl (R.P.), gertjan.veenstra@ru.nl (G.J.C.V.)
https://doi.org/10.1016/j.stemcr.2025.102422

SUMMARY

Stem cell-based models of human heart tissue and cardiac differentiation employ monolayer and 3D organoid cultures with different properties, cell type composition, and maturity. Here we show how cardiac monolayer, embryoid body, and engineered heart tissue trajectories compare in a single-cell roadmap of atrial and ventricular differentiation conditions. Using a multiomic approach and gene-regulatory network inference, we identified regulators of the epicardial, atrial, and ventricular cardiomyocyte lineages. We identified *ZNF711* as a regulatory switch and safeguard for cardiomyocyte commitment. We show that *ZNF711* ablation prevents cardiomyocyte differentiation in the absence of retinoic acid, causing progenitors to be diverted more prominently to epicardial and other lineages. Retinoic acid rescues this shift in lineage commitment and promotes atrial cardiomyocyte differentiation by regulation of shared and complementary target genes, showing interplay between *ZNF711* and retinoic acid in cardiac lineage commitment.

INTRODUCTION

The first precursor cells of the heart emerge during early gastrulation when the three germ layers of the embryo are formed (Lescroart et al., 2014). These progenitor cells reside within the splanchnic lateral mesoderm in spatially segregated populations, notably the first and the second heart field (FHF and SHF), which together will form the cardiac crescent (Buckingham et al., 2005). These progenitor states have been studied using single-cell omics approaches in mouse embryonic tissues, as reviewed recently (Lescroart and Zaffran, 2022). The lineages of the FHF primarily populate the left ventricle and part of the atria. The SHF is divided into an anterior and posterior section (aSHF and pSHF), which are transcriptionally distinct and contribute to different parts of the developing heart. The aSHF forms the right ventricular myocardium and outflow tract (OFT), whereas progenitors of the pSHF commit to the atrial lineage under the influence of retinoic acid (RA) signaling (Protze et al., 2019). Reports on cardiac development in humans start at five weeks of gestation, when the heart already features multiple chambers (Asp et al., 2019; Cui et al., 2019; Farah et al., 2024; Sahara et al., 2019). By that time, the multipotent cardiac progenitors have produced the cardiomyocyte (CM), endothelial, epicardial, and smooth muscle lineages and have built a myocardium that forms the atria and ventricles (Protze et al., 2019). Very little is known about the earliest stages and distinctive lineage choices of human cardiac development *in vivo* (Tyser et al., 2021; Zeng et al., 2023).

Human pluripotent stem cells (hPSCs) can differentiate to many cell types *in vitro*, thus presenting a relevant alternative for the early steps of human tissue development (Takahashi et al., 2007; Thomson et al., 1998; Yu et al., 2007). Various culture models have been established to obtain CMs (Devalla and Passier, 2018), with variations including RA treatment to enrich for atrial CMs (aCMs) (Schwach et al., 2022; Zhang et al., 2011) or epicardial derivatives (Hofbauer et al., 2021; Meier et al., 2023). Over time, the cardiac cultures have increased in complexity leading to advanced maturity of the CMs and simultaneous development of a dynamic pool of cardiac cell types (Kannan et al., 2021).

Single-cell transcriptomic studies have elucidated the differentiation processes of hPSCs toward CMs (Ameen et al., 2022; Grancharova et al., 2021; Hofbauer et al., 2021; Lescroart and Zaffran, 2022; Meier et al., 2023). Several of these studies highlighted the presence of non-myocyte subpopulations within the culture (Churko et al., 2018; Mononen et al., 2020), while others shed light on the specification of particular CM subtypes, such as atrial, right and left ventricular CMs, and node-like CMs (Pezhouman et al., 2021; Wiesinger et al., 2022; Yang et al., 2022). However, very little is known about how cardiac multipotent

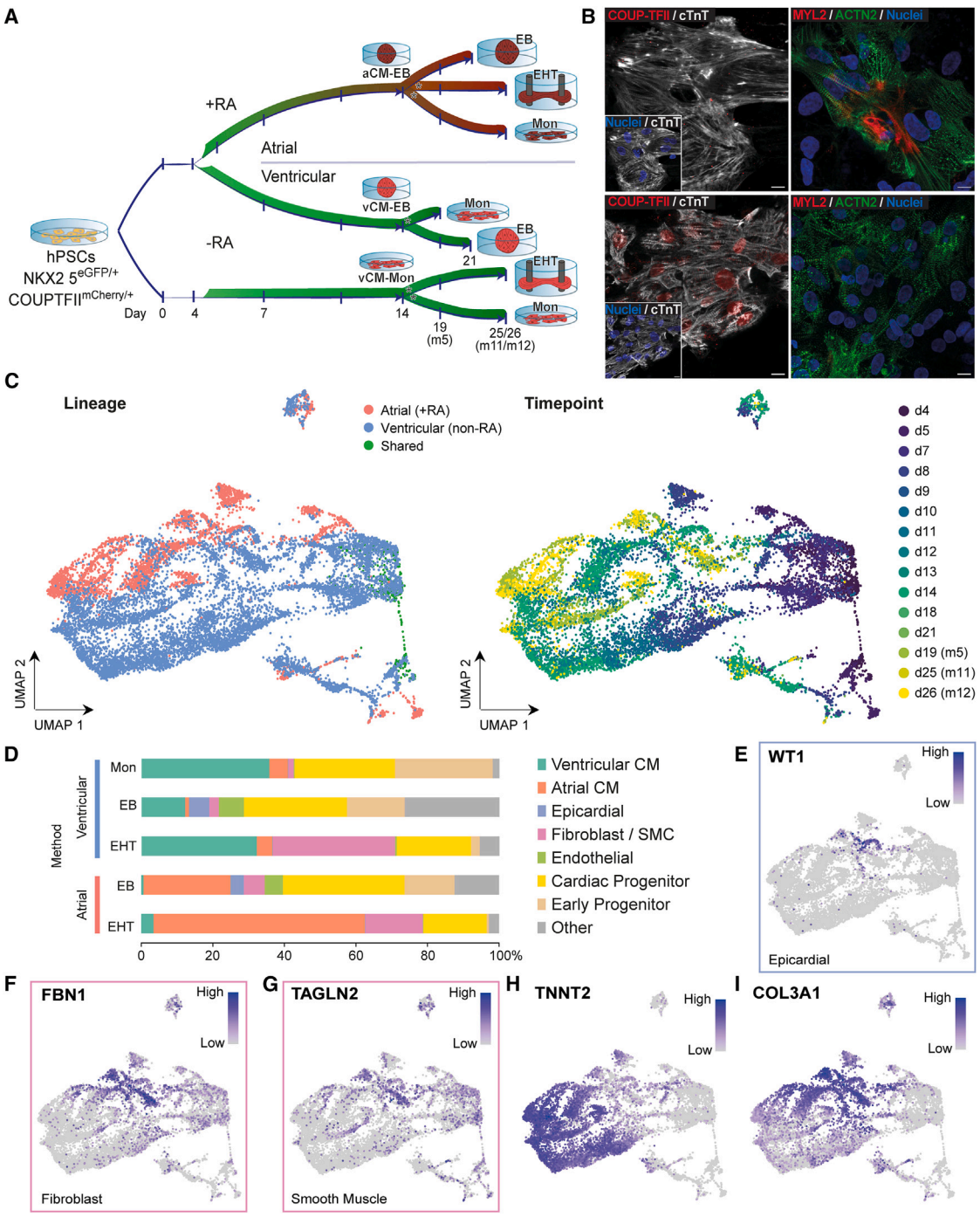

Figure 1. Single-cell atlas of human cardiac differentiation in monolayer, embryoid body, and engineered heart tissue cultures

(A) Schematic representation of the hPSC-derived cardiomyocyte (CM) differentiation cultures. hPSCs were differentiated in monolayer (Mon) or embryoid body (EB) cultures over the course of 14 days. At day 14, sorted CMs and non-CMs were replated in engineered heart tissues (EHTs) or replated as monolayers for comparison of the 3D culture (indicated with stars), while the EBs were kept in culture until day 21 (see Figure S1 for a detailed overview). RA, retinoic acid; d1–d21, day 1–21; m5–m12, day 5–12 in maturation medium (day 14–26; EHT and monolayer only). This single-cell atlas is based on four independent multi-well differentiation experiments, with each culture protocol (Mon, EB, and EHT) and culture condition (+/− RA) covered by at least two independent experiments. In one experiment all protocols and conditions were sampled in parallel (see methods). Cell states were highly consistent between experiments and time points (Figure S2F).

(legend continued on next page)

progenitors give rise to different CM and non-myocyte lineages and how this is regulated. Hence, there is a need for disentangling the gene-regulatory networks (GRNs) of cardiac development as the cells commit to specific lineages and how this relates to *in vitro* culture conditions. Understanding these mechanisms will aid in the advancement of cardiac hPSC models and their ability to more accurately model cardiovascular development and heart disease.

Here we present a detailed comparison of *in vitro* cardiac differentiation conditions from hPSCs using single-cell transcriptomic (RNA-seq) and chromatin accessibility (Assay for Transposase-Accessible Chromatin; ATAC-seq) data, which we used to construct a roadmap of atrial and ventricular multilineage differentiation. We used a combination of monolayer, embryoid body (EB), and engineered heart tissue (EHT) cultures to compare their cellular compositions and differentiation stages. In addition, we used RA to compare multilineage differentiation in atrial and ventricular cultures. Direct comparisons between the cardiac models revealed subpopulations resembling fetal cell states and identified transcriptional regulators at the onset of lineage commitment. The integrative multiomic approach led to the identification of *ZNF711* and the interplay of this zinc finger with RA in balancing commitment to the CM and epicardial lineages.

RESULTS

CM differentiation methods produce cardiac cell states found in the human fetal heart

To compare the early steps of cardiac lineage development, we differentiated dual fluorescent *NKX2-5*$^{EGFP/+}$ and *COUP-TFII* (*NR2F2*)$^{mCherry/+}$ hPSCs (Schwach et al., 2017) to CMs under CM monolayer (Mon) and cardiac EB conditions, with or without RA (see methods and Figures 1A and S1A). We and others showed previously that RA redirects differentiation toward aCMs (Devalla et al., 2015; Schwach et al., 2017, 2022; Zhang et al., 2011), which occurs at high efficiency as evaluated by fluorescence-activated cell sorting (Figure S1B). At day 14, CMs of these cultures were further matured for an additional 12 days (m12; until day 26) in CM maturation medium, either as 3D EHTs (Birket et al., 2015; Ribeiro et al., 2022) or as replated monolayer cells that served as a control for the changes that occur in the EHTs (Figure S1C). The atrial and ventricular CMs expressed the expected regional markers (NR2F2 and MYL2 respectively; Figure 1B) in addition to general CM markers (MYL7 and ACTN2; Figure S1D), while displaying typical action potential profiles, with higher frequencies and shorter action potential duration times in aCMs (Figure S1E). Continued culture of the CMs in the EHT model enhanced their respective identities, as shown by immunohistochemistry of aCM- and ventricular CM (vCM)-specific markers (Figure S1F). Additionally, the EHTs showed robust contraction forces (around 100 μN; Figure S1G) as expected from functional CMs matured in EHTs (Ribeiro et al., 2022). Moreover, the EHTs showed patterns of gene expression (Figure S1H) reflective of CM maturation (Harlaar et al., 2022).

To produce a detailed map of how cardiac progenitors give rise to CMs and other cardiac cell types, we performed single-cell RNA sequencing (RNA-seq) on samples of different culture methods and time points (Figures 1A–1C, S1A, and S1C). We used a 384-well plate sorting-based platform (SORT-Seq) because of the flexibility it offers in experimental design, and it facilitates the capture of many time points and different culture conditions (Hashimshony et al., 2016). Particularly, we captured cells at the mesodermal stage (day 4–5), cardiac progenitors (day 7–9), cells committed to the CM fate (day 10–14), and definitive CMs (day 18–26). This resulted in a single-cell landscape with a total of 12,706 cells after filtering for quality (see methods and Figures S2A and S2B). Known cardiac markers for different stages of development were evaluated for their overall expression patterns over time (Figure S2C), indicating a decrease in mesodermal markers (*MIXL1* and *PDGFRA*) and an increase in cardiac progenitor markers (*MEF2C* and *NKX2-5*), followed by expression of structural CM genes (*TNNT2* and *MYL7*) and either atrial (*KCNA5*, *KCNJ3*, and *VSNL1*) or ventricular (*MYL2*, *MYH7*, and *VCAM1*) CM genes (Figures S2C and S2D).

To predict which cells of the different culture methods represent a similar biological state, we integrated the data using an unsupervised selection of mutual cell pairings across the multiple culture experiments (Figures S2E and S2F) (Hao et al., 2021). This resulted in an integrated *in vitro* cardiac differentiation atlas, in which a chronological progression of time points and cell states was observed, while

(B) Immunohistochemistry of atrial (COUP-TFII/NR2F2), ventricular (MYL2), and general CM (cTnT and ACTN2) marker genes in day 14 vCM (top row) and aCM (retinoic acid treated; bottom row) culture conditions. Scale bar, 10 (COUP-TFII/cTnT) and 20 μm.
(C) Single-cell temporal atlas Uniform Manifold Approximation and Projection (UMAP) labeled with culture conditions (left) and harvest time point (right).
(D) Proportions of the different cell states per culture method. Cell states annotation process is shown in Figures S3 and S4.
(E–G) Cell type marker expression levels visualized onto the atlas UMAP, with *WT1* as epicardial, *FBN1* as fibroblast, and *TAGLN2* as smooth muscle marker.
(H and I) Inversely related expression patterns of *TNNT2* (F) and *COL3A1* (G) visualized onto the atlas UMAP.

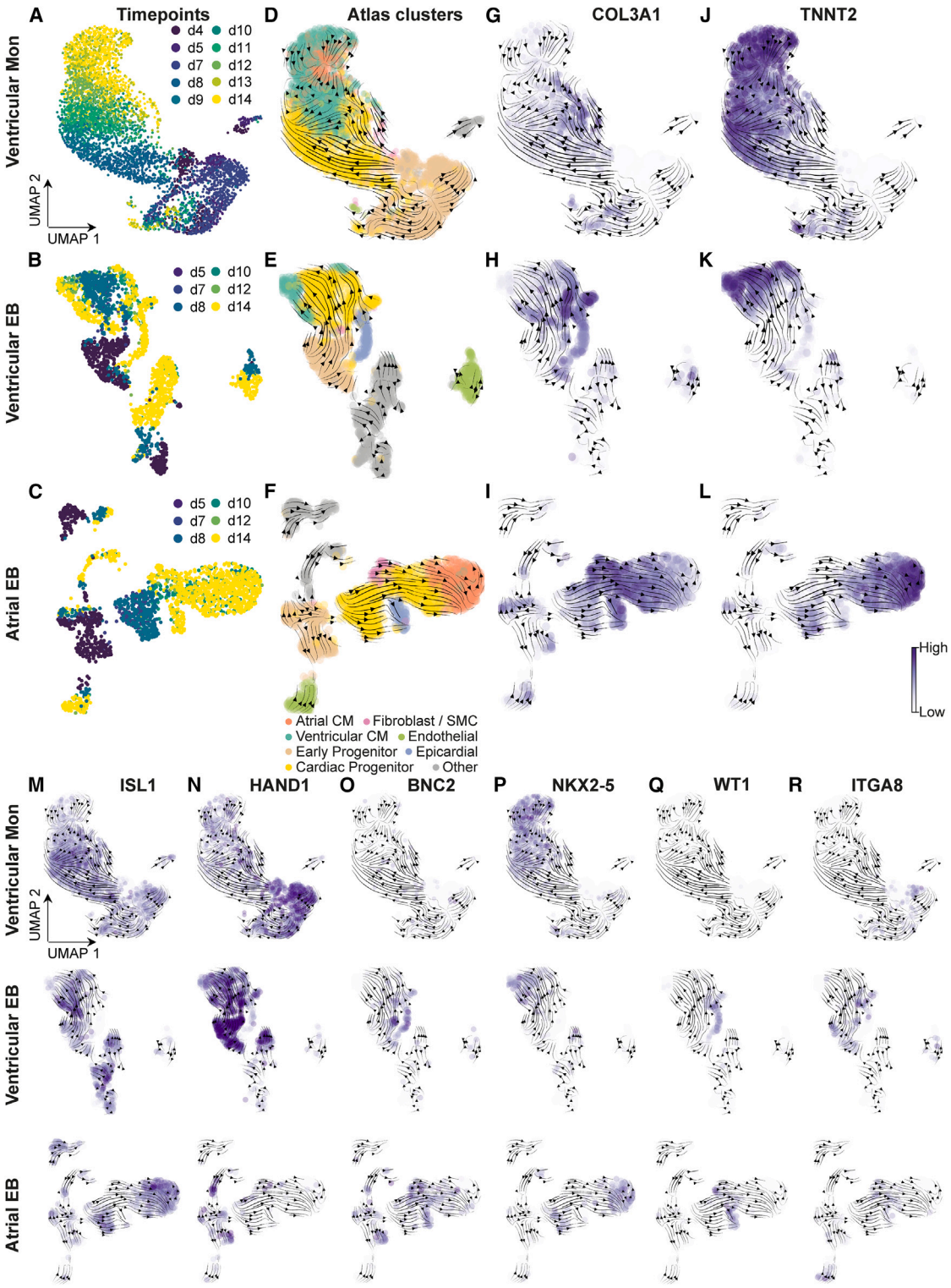

Figure 2. Trajectories of cardiac progenitor differentiation in EB and monolayer cultures

UMAP representations of early time point (day 4 to day 14) subsets of the atlas per culture protocol (top, middle, and bottom row representing, respectively, the vCM-mon, vCM EB, and aCM EB protocols).

(legend continued on next page)

resolving distinctions between the atrial and ventricular lineage (Figure 1C). Comparing the end states of the differentiation culture methods revealed a clear shift of the definitive CM populations between monolayer and EHT cultures, corresponding to further maturation upon culturing as 3D EHTs (Figure S2G). To annotate the cell states in this atlas, we compared the cell clusters with an integrated dataset of human fetal heart development (Asp et al., 2019; Cui et al., 2019) (Figures S3A–S3C). This comparison revealed that, in EBs from day 8 onward, clusters matching cardiac fibroblasts and smooth muscle cells were present (clusters 15 and 16), alongside clusters comparable to endothelial and epicardial cells (respectively clusters 17 and 22) (Figures 1D, S3D, and S4A–S4C). Fibroblasts (cluster 16) were relatively abundant in the EHT model, but epicardial-like cells (cluster 22) were not (Figures 1D and S4A–S4C). This decrease is likely linked to the dissociation of the EBs and subsequent formation of EHTs (Figure S1C). Expression of well-known marker genes, such as *FBN1* for fibroblasts, *WT1* for epicardium, and *TAGLN2* for smooth muscle cells (Figures 1E–1G), further confirmed the presence of these non-myocyte cell types. Lastly, one set of clusters (clusters 10, 13, 18, and 25) present in the EB cultures (Figure S4C) was found enriched for markers of endoderm-committed cell types, such as early foregut progenitors (Figure S4D) (Ang et al., 2018; Scheibner et al., 2021). The presence of these endoderm derivatives can contribute to epicardial and myocardial lineage development (Branco et al., 2022). Overall, these data highlight the broad lineage potential in both ventricular and atrial EB cultures (Figure 1D). In addition, we found that a population of cells consisting of non-CM and early CM progenitors was marked by high expression of *COL3A1* and that this expression is inversely related to that of *TNNT2* in the CM lineage (Figures 1H and 1I). This *COL3A1*-high population shows a different abundance in the cardiac cultures, raising the possibility that the balance of lineage commitment of multipotent progenitors toward CM and non-CM identities is affected by the culture method.

Early trajectories show expression patterns mimicking *in vivo* development

To study the relationship between *COL3A1*-high progenitors and the CM and non-CM lineages, we performed cell trajectory analysis for each culture method from early time points up to day 14 (Figures 2A–2F). This revealed the progression of cardiac progenitors expressing *COL3A1* (Figures 2G–2I) to *TNNT2*-positive CMs in all cultures (Figures 2J–2L) and epicardial cells in atrial and ventricular EBs (Figures 2D–2F and 2M–2R). The epicardial trajectory is supported by the presence of cells expressing *ISL1*, *HAND1*, and *BNC2*, markers of the juxta-cardiac field or pre-epicardial progenitor state (Figures 2M–2O). This population continued to develop into cells negative for *ISL1* and *NKX2-5*, while expressing epicardial markers *BNC2*, *WT1*, and *ITGA8* (Figures 2M, 2O, 2P, and 2Q). In each of the early cultures, the *COL3A1*-high state was present, although this was more pronounced in the atrial EBs treated with RA (Figure 2I). In the ventricular monolayer culture, CM progenitors can go through either a high or a low *COL3A1*-expression state before acquiring the CM identity (Figures 2G and 2J). In EBs, the progenitors are routed almost exclusively through a *COL3A1*-high state (Figures 2H and 2I), but the *COL3A1* is more persistent in the RA-treated atrial EB cultures. In most progenitors present in the EBs, *COL3A1* appears to be co-expressed with the SHF progenitor marker *ISL1* (Figures 2H, 2I, and 2M). There is no co-expression, however, in the epicardial population, which does express *COL3A1* but not *ISL1* (Figures 2H, 2I, and 2M). This is in line with previously described dynamics of *ISL1* expression during epicardial lineage progression (Meier et al., 2023).

To establish if other *in vivo* developmental stages were recapitulated *in vitro*, we checked the expression of SHF and FHF markers across culture methods and time points (Figures S5A and S5B). Several SHF markers were upregulated over the course of differentiation in both the atrial and ventricular lineage (*HAND2*, *ISL1*, and *FOXC1*; Figure S5B). In the atrial EB culture conditions, an increase of *TBX5* expression occurred directly after a transient increase of *HOXA1* expression (Figure S5B). This expression profile is consistent with the pSHF identity (Protze et al., 2019; Roux et al., 2016; Steimle and Moskowitz, 2017; Sweat et al., 2023). Other examples of pSHF markers that increased in the atrial EBs are *FOXF1*, *TBX18*, and *OSR1* (Meilhac and Buckingham, 2018; Steimle and Moskowitz, 2017) (Figure S5C). On the other hand, the vCM cultures

(A–C) UMAPs labeled with time points (d4–d14, days of differentiation). For experimental design and replicates, see Figures 1 and S1 and methods.

(D–F) UMAPs labeled with cell states (cf. Figures 1D and S3B).

(G–L) (G–I) and (J–L) UMAPs with the expression values of, respectively, *COL3A1* and *TNNT2*.

(M–R) UMAPs with the expression values of the SHF marker *ISL1* (M), pre-epicardial genes *HAND1* (N), *BCN2* (O), and *NKX2-5* (P) and epicardial markers *WT1* (Q) and *ITGA8* (R).

Arrows (D–R) show cell state dynamics predicted by RNA velocity (see methods). Discontinuities visible in the EB UMAPs indicate an early lineage separation of the endothelial and "other" lineage present in the cultures. Atrial EBs show an additional separation directly after day 5 where the cells were treated with retinoic acid, which causes a rapid and relatively large change in gene expression.

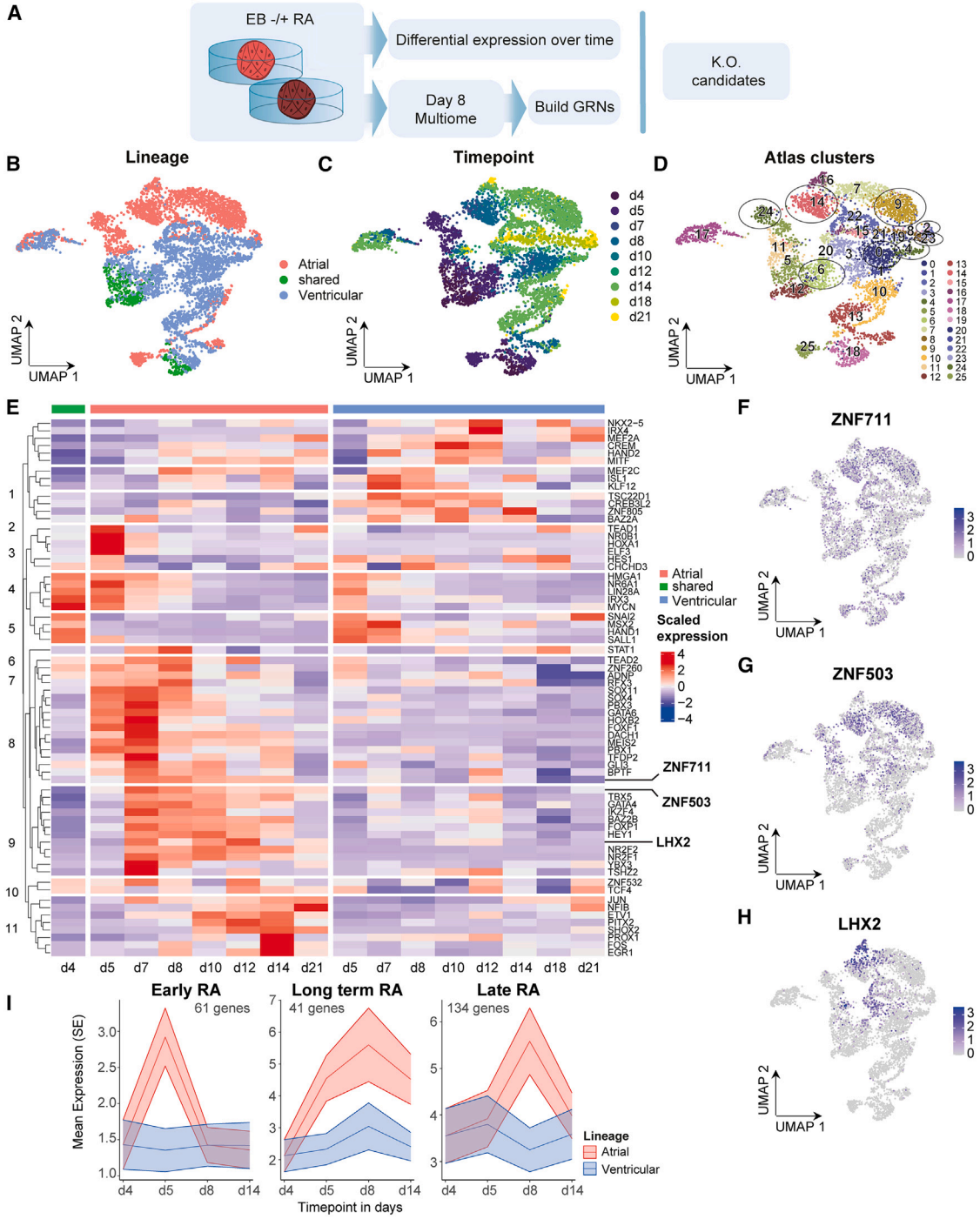

Figure 3. Transcription factor analysis in the EB atlas subset

(A) Overview of the approach to select transcription factors (TFs) of interest in the +RA/non-RA-treated EBs. Differentially expressed TFs were determined over time across the aCM- and vCM-committed cell clusters in the EB subset of the atlas from two independent differentiations. Multiome analysis (snRNA-seq and snATAC-seq from the same nuclei) of day 8 +RA/non-RA-treated EB cultures was used to generate cell type-specific gene-regulatory networks (GRNs). The combination of these approaches identified potential knockout candidates.

(B and C) UMAP representation of the EB subset of the atlas. Cells labeled according to lineage (B) and harvest time point (C) with $n = 2$ for day 4, 5, 8, and 14, from separate differentiation experiments.

(legend continued on next page)

showed limited expression of *TBX5* in comparison to the aCM cultures (Figure S5B), while *FGF10* and *FGF8* increased alongside an early expression of *SIX1*, indicative of aSHF identity (Itoh et al., 2016; Yang et al., 2022) (Figure S5D). By examining the identity of the CMs from day 14 onwards (Figure S2D), we observed a higher expression of *MYL2*, together with the expression of *HAND2* and *SEMA3C* (Figures S5B and S5E) in the ventricular clusters (derived from both EB and monolayer cultures), associated with an OFT-like or right ventricle CM identity (Rana et al., 2014; Yang et al., 2022). These findings suggest a predominantly aSHF identity in the ventricular EB culture and a posteriorizing effect of RA (pSHF) in the atrial EB culture. The ventricular cultures additionally expressed the FHF marker *HAND1* (Figure S5B). Collectively, these results outline multiple routes toward a CM fate, one with relatively low *COL3A1* expression on a mixed aSHF-FHF trajectory toward vCMs and another of *COL3A1*-high expression progressing toward aCMs, derived from a posteriorized SHF lineage driven by exposure to RA (Figure S5C). Interestingly, epicardial marker genes such as *SFRP5* overlapped with *COL3A1* in the non-CM branches in EB cultures, irrespective of RA-induced posteriorization of the SHF (Figures S4B and S5F). These data document the dynamic re-routing of progenitors along developmental trajectories depending on the culture method, raising the question what molecular mechanisms are underlying this plasticity of multilineage cardiac differentiation.

Identification of candidate cardiac regulators by integrative multiomic analysis

We focused first on the influence of RA on lineage specification in EBs, as it provides a major switch for atrial versus ventricular CM lineage specification in these cultures, in the presence of a relatively stable number of non-CM cell types (cf. Figure 1D). To study lineage-specific transcription factor expression patterns, an EB subset of the atlas was generated to perform differential expression testing over time on CM-committed cell clusters (Figures 3A–3D). This analysis outlined several known CM-specification regulators, such as *IRX4*, *IRX3*, and *HES1* for vCM and *MEIS2*, *NR2F2/1*, and *HEY1* for aCM (Figure 3E). Additionally, atrial-enriched expression was found for *LHX2*, *ZNF711*, and *ZNF503* (Figures 3F–3H), genes that are not known for their role in CM lineage commitment. Additionally, while *ZNF711* showed broad expression across both lineages, RA appeared to further induce this zinc-finger gene in the atrial lineage in a temporal manner (Figures 3E and 3F). Since RA was added to the atrial cultures for 24 h on day 4, "early" genes can be identified that are only transiently induced by RA (for example *HOXA1*), whereas "long-term" genes (for example *LHX2*, *ZNF711*, and *ZNF503*) are induced with delayed dynamics (Figures 3E and 3I).

To examine the role of these and other transcription factors at the level of chromatin accessibility, we generated an orthogonal single-nucleus multiomic dataset (snRNA-seq and snATAC-seq, both modalities measured from the same nuclei) of atrial and ventricular EBs at the onset of lineage commitment (day 8, Figures 3A and 4). Dimensionality reduction and clustering of the transcriptome modality of the data led to the identification of the cell states we identified before, with a *KCNJ3*- and *NR2F1*-positive population of early aCMs, vCMs expressing *MYL7* and *MYH6*, a *GRHL2*- and *CDH1*-positive population of epicardial cells, and an endothelial cluster marked by *KDR* (or *FLK1*) and *FLI1* expression (Figures 4A. 4B, and S6). CM subclusters vCM2 and aCM2 were marked by gene expression associated with different cell-cycle phases (Figures S6B and S6C). Correlation of the multiome clusters with day 8 EB clusters of the atlas revealed similarities of multiome clusters 4 and 8 with the other/endoderm populations of the atlas (Figures 4A and S7, atlas cluster), while also expressing fibroblast genes *FGF13* and *SCN7A* (Figure S6C).

For these clusters, we used the chromatin accessibility modality of the multiomic dataset to perform peak calling (150,597 peaks with chromatin accessibility; Table S1) and differential peak accessibility analysis (672 differential peaks; Table S1 and Figure S6D). At this early stage of lineage commitment and RA-dependent change, quantitative differences in accessibility between cell clusters were observed for relatively few genes (Figures 4C and S6D). We identified the motifs contributing to these differences in chromatin accessibility between cell types, based on regression analysis ("motif activity," see methods). We identified motifs linked to important cardiac regulators (Figure 4D and Table S2); for example, the motifs of RA receptor beta (RARB) and HOXB1 are associated with

(D) UMAP with cluster labels. Circles indicate the clusters used in differential gene analysis between the aCM and vCM trajectories over time. Comparisons were performed between cluster 24 and 6, cluster 14 and 0, cluster 9 and 4, and cluster 2 and 23.
(E) Differentially expressed genes between early and late CM clusters, outlined in (D), across the two lineages within the EB subset.
(F–H) Hits of interest from (E), *ZNF711* (F), *ZNF503* (G), and *LHX2* (H) with their expression levels onto the EB subset UMAP.
(I) Average expression levels over time per gene set found differentially upregulated in atrial versus ventricular culture, subdivided into an early RA-responsive (left), a long-term RA-responsive (middle), and late RA-responsive subset (right) (see methods; gene lists in Table S2).
d, day of culture; d4 is shared between the lineages; d5, the first day after RA treatment in the atrial culture; SE, standard error.

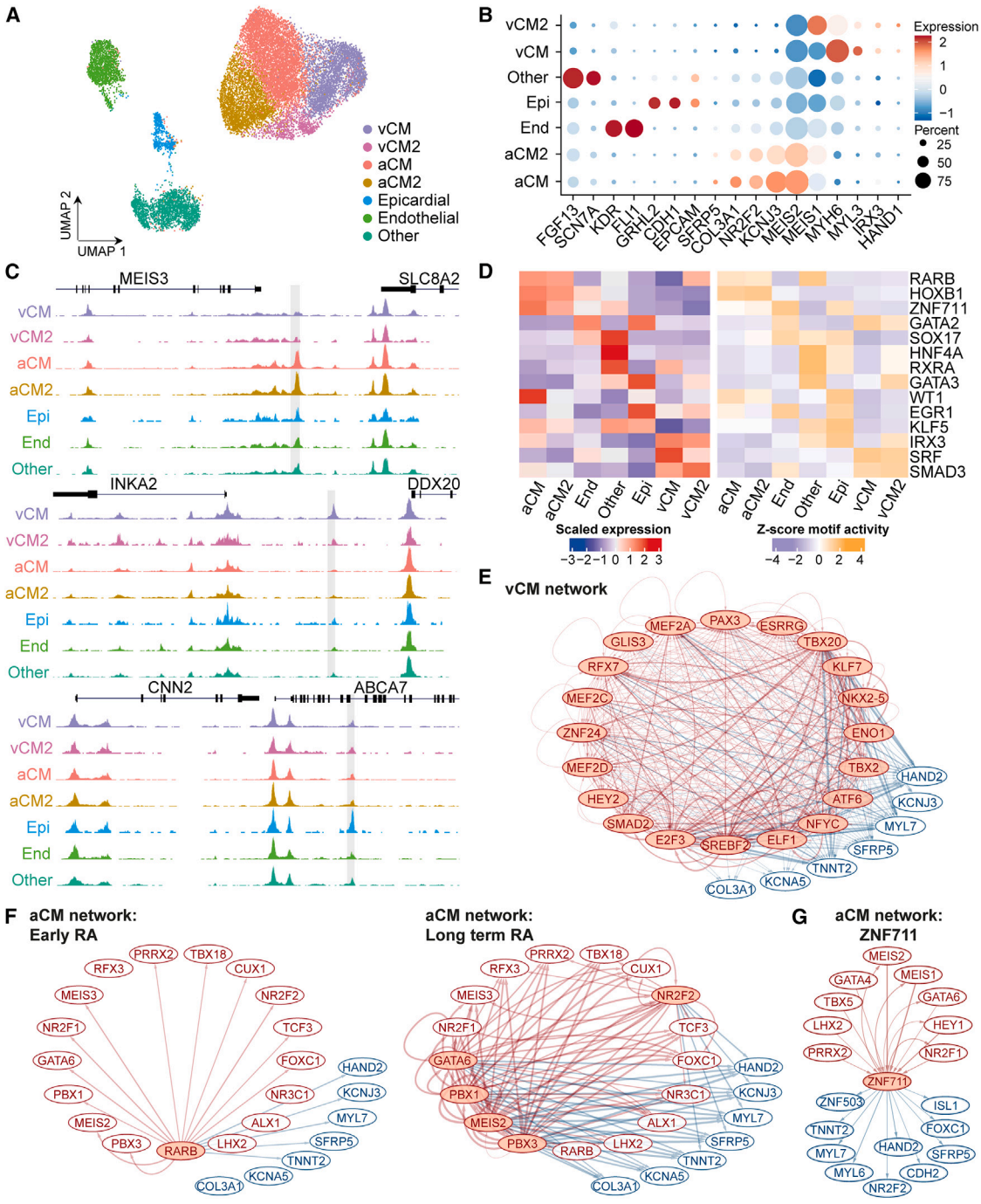

Figure 4. Identification of candidate transcriptional regulators with multiome data

(A) UMAP representation of multiome data from day 8 EBs directed to the atrial and ventricular lineage. Dimensionality reduction and clustering were performed on the scRNA-seq fraction.

(B) Scaled marker gene expression levels over the different cell states. End, endothelial; Epi, Epicardial.

(C) Cluster pseudobulk scATAC-seq signals, zoomed in on three different loci in Genome Browser view, where a differentially accessible (DA) peak was found enriched in the atrial (top), ventricular (middle), or epicardial (bottom) cluster, between the *MEIS3* and *SLC8A2* gene (top), *INKA2* and *DDX20* gene (middle), and within the *ABCA7* gene (bottom). The gray box highlights the 200 bp peak, differential in signal across the clusters. Black boxes within the genes indicate exons.

(legend continued on next page)

chromatin accessibility in aCMs (aCM and aCM2 clusters). The motifs for IRX3 and SRF, important for aSHF and CM differentiation (Guo and Pu, 2020; Kim et al., 2016; Yang et al., 2022), were associated with the vCM clusters. Other examples include the WT1 and EGR1 motifs enriched in the epicardial cluster (Meier et al., 2023), the GATA2 motif in endothelial cells (Kanki et al., 2011), and motifs for HNF4A and SOX17 in the other (or endoderm-like) cluster (Hanawa et al., 2017; Kanai-Azuma et al., 2002). A motif for ZNF711 was associated with increased accessibility in the endothelial, epicardial, and aCM clusters (Figure 4D). Performing this regression-based analysis on all peaks (instead of differential peaks) showed motifs for similar transcription factors, with motifs for HOXB1 and RARB (aCM chromatin accessibility), SRF (vCM), HNF4A (other), and GATA2 (endothelial), and further down the list also motifs for EGR1 and WT1 scoring high for epicardial chromatin accessibility (Table S2).

GRN downstream of RA

To understand the transcriptional regulation driving CM specification in these stages of cardiac development, we predicted the CM-specific GRNs utilizing scANANSE, a recently developed tool for identification and prioritization of key transcription factors involved in cell fate determination (Smits et al., 2023). In short, scANANSE prioritizes transcription factors by integration of chromatin accessibility (sequence motif content) and transcriptome data, inferring a differential network between two biological states. To generate these networks, we used the complete peak set as input for scANANSE (Table S1). The predicted aCM network (Table S2) highlighted many regulators known for their role in cardiac development and regulation of cardiac progenitors from the pSHF, like *TBX18*, *MEIS2*, and *NR2F2* (Lescroart and Zaffran, 2018; Quaranta et al., 2018). The vCM network included multiple known CM regulators, such as *TBX20*, *MEF2A/C*, and *NKX2-5*, but also *HEY2*, a regulator particular to the ventricular subtype (Churko et al., 2018) (Figure 4E and Table S2). For the non-CM clusters, which consisted of cells from both culture conditions, we compared the cell type-specific network to an average network of all cells together (see methods). Top influential factors were *GRHL2*, *TFAP2A*, and *BACH2* for the epicardial network; *ERG*, *ETS1*, *FLI1*, and *ELK3* for the endothelial network; and *RFX6*, *GATA3*, *HNF4A*, and *HNF4G* for the endoderm network (Table S2).

Subsequently, we used the temporal gene expression information from our transcriptome atlas (Figure 3I and Table S2) to infer a temporal regulatory hierarchy within the aCM network. Based on these expression dynamics within the top-ranked network of transcription factors, RARB emerged as the regulatory starting point (Figure 4F, left), consistent with the use of RA to trigger atrial lineage commitment. RARB is predicted to regulate multiple well-known pSHF genes (i.e., *MEIS2*, *TBX18*, *NR2F2*, and *FOXC1*). Top regulators encoded among the long-term RA-induced genes are *GATA6*, *MEIS2*, *PBX3*, *PBX1*, and *NR2F2* (Figure 4F, right). The predicted regulatory interactions of seven genes of interest (*COL3A1*, *KCNA5*, *TNNT2*, *SFRP5*, *MYL7*, *KCNJ3*, and *HAND2*) suggest that most targets can be regulated by RARB directly, whereas *COL3A1* and *KCNA5* may be regulated further downstream in the network by long-term regulators.

Among the influential factors of the aCM network, also ZNF711 and LHX2 were identified. Multiple factors were predicted to regulate *ZNF711* (Figure 4G), among which are known pSHF factors TBX5, HEY1, MEIS1/2, and NR2F1 but also factors more generally implicated in cardiac development such as GATA4/6 (Xin et al., 2006). ZNF711 was predicted to regulate SHF genes *ISL1* and *FOXC1* and aCM-specific markers *NR2F2* and *MYL6*. Interestingly, ZNF711 was also predicted to regulate general CM genes, i.e., *TNNT2*, *MYL7*, and *N-cadherin* (*CDH2*). Additionally, *ZNF503* was found downstream of ZNF711 in the aCM network. These findings were especially interesting since limited information is available regarding the potential role of these zinc-finger proteins in cardiac development. The highly conserved *ZNF503* protein has been shown to transcriptionally repress *GATA3* (Shahi et al., 2017) and to play a critical role during embryonic development in mice and zebrafish (Boobalan et al., 2022; Nakamura et al.,

(D) Motif enrichment as identified by Maelstrom analysis on the DA peaks (Table S1) clustered on accessibility signal (Figure S6D). Full Maelstrom analysis results are shown in Table S2. Left heatmap shows expression levels of binding TFs, and right heatmap shows the linked motif activity as inferred with motif analysis.

(E) Differential network of the vCM over the aCM cluster, as predicted by scANANSE. Top 20 most influential transcriptional regulators (red) and 7 markers of interest (blue) are shown.

(F) Differential network of the aCM over the vCM cluster, as predicted by scANANSE. Top 20 most influential regulators (red) and the same targets (blue) as in (E) are shown. Nodes in the network are filtered for temporal expression, showing the early RA responding gene RARB and the connections to its targets (left) and the long-term RA responding genes and their target interactions (right). Highlighted nodes indicate presence of these regulators in an RA-responsive subset (Figure 3I and Table S2).

(G) Subset of the aCM network for ZNF711, with selected upstream factors from the aCM differential network (red) and targets of interest downstream of ZNF711 (blue).

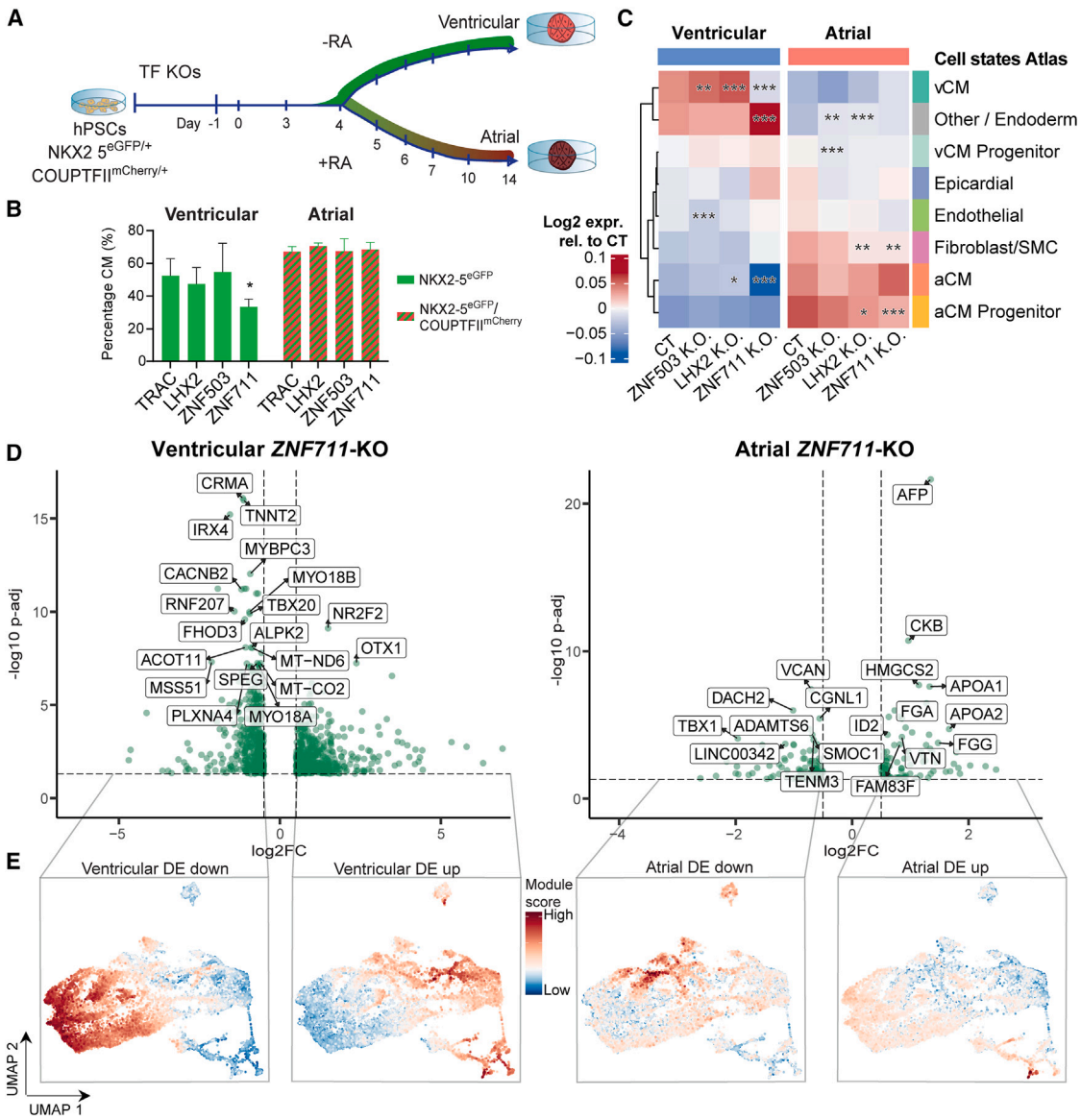

Figure 5. Knockout experiments for LHX2, ZNF711, and ZNF503

(A) Experimental setup for the transcription factor (TF) knockout (KO) experiments. hPSCs with the *TRAC* (control), *ZNF711*, *ZNF503*, or *LHX2* knockout (TF KOs) were differentiated toward aCM- and vCM-EBs (+/− RA, respectively). At day 14 of differentiation, EBs were collected for subsequent analysis.

(B) Percentages of CMs per KO measured in cells positive for the CM reporters NKX2-5 in ventricular (non-RA-treated) and NKX2-5 and NR2F2 in atrial (+RA-treated) cultures at day 14. *TRAC*-KO is the gene CRISPR control. Data are mean ± SEM; ordinary two-way ANOVA with Tukey's multiple comparisons test; ***p*-adjusted < 0.001, vs. *TRAC* ($n = 3$ independent differentiations per culture protocol and KO target).

(C) Averaged cell lineage expression scores within the *ZNF503*, *LHX2*-KO, *ZNF711*-KO, and TRAC control relative to the average of the TRAC controls from both lineages. Expression scores were based on the top 200 marker genes per cell type (day 14 EB, Table S3). Relative expression scores can be compared between ventricular (left) and atrial (right) panels. Within each panel, scores should be compared to its own control (CT) of the same panel. Significance was calculated over the averaged expression levels across 200 genes and per matched replicate and control. Stars indicate significance of the highest *p* value found among the replicates of a condition (see methods; **p*-adjusted < 0.05, ***p*-adjusted < 0.001, and ****p*-adjusted < 0.0001).

(D) Volcano plot of the differentially expressed (DE) genes of the *ZNF711*-KO cells cultured toward vCMs (non-RA, left) and aCMs (+RA, right) (adjusted *p* value < 0.05). Text labels show top hits with the lowest adjusted *p* value. Vertical dotted line indicates |log2FC| > 0.5, and horizontal dotted line indicates |−log10*p* value| < 0.05.

(legend continued on next page)

2008). Our network predictions and the temporal and RA-induced expression patterns of *ZNF711* and *ZNF503* prompted us to test the function of these little-known zinc-finger factors in cardiac differentiation.

Ablation of ZNF711 halts CM differentiation and favors the epicardial and endodermal lineages

We selected three genes (*LHX2*, *ZNF711*, and *ZNF503*) to assess their roles in cardiac lineage commitment. For each of these factors, a CRISPR knockout (KO) was performed in the dual NKX2.5$^{EGFP/+}$COUP-TFII (NR2F2)$^{mCherry/+}$ hPSC reporter line (Figure 5A), with KO efficiencies over 70%, both before and after cardiac EB differentiation (Figures S8A and S8B). KO hPSCs were immediately differentiated in EB cultures over the course of 14 days toward the ventricular (non-RA) and atrial (+RA) cardiac cell types. The efficiency of CM differentiation was assessed using NKX2-5-driven GFP reporter expression (Figure 5B). In the ventricular *ZNF711*-KO culture, reporter expression was significantly lower compared to control (*TRAC*), while this was not observed in the RA-treated (atrial) *ZNF711*-KO EBs or in any of the other conditions. The lower CM differentiation efficiency in the ventricular *ZNF711*-KO was accompanied by an increase in the abundance of NKX2-5-GFP-negative and NR2F2-mCherry-positive fraction compared to control (Figures S8C and S8D), suggesting a shift in lineage commitment.

A substantial differentiation defect in the ventricular culture was corroborated by transcriptome analysis, which we performed for both the atrial and ventricular cardiac EB cultures of each KO at day 14 of differentiation. The strongest changes in gene expression were detected in the *ZNF711*- and *LHX2*-ablated cultures relative to controls (Figure S8E). To explore changes in cell type commitment, sets of 200 marker genes per cell type were defined from the atlas (Table S3) to calculate average cell type-specific marker expression levels per KO and culture condition (Figure 5C). These lists included *ANGPT1*, *PPP1R12B*, *ATP2A2*, and *TTN* as top aCM markers, whereas *NEBL*, *TTN*, and *VCAM1* were among the ventricular CM markers. Other markers include *MYCT1*, *CDH5* (*VE-Cadherin*), *CD93*, and *PECAM1* (*CD31*) for the endothelial cluster; *NR1H4* (*FXR*), *DCN* (*Decorin*), and *POSTN* for the fibroblast/smooth muscle cell population; and *WT*, *BNC1*, and *KRT18* for the epicardial cluster. This analysis uncovered that changes in cell lineage-specific markers were highly dependent on the treatment with RA. The *ZNF711*-KO samples showed a significant decrease in both aCM and vCM markers under ventricular conditions (Wilcoxon p-adjusted 2.7×10^{-9} and 2.2×10^{-11}, respectively). In RA-treated atrial cultures, however, vCM marker expression was not affected significantly, while the expression of aCM progenitor markers was reduced (Wilcoxon p-adjusted 2.6×10^{-11}). In ventricular cultures, definitive endoderm marker expression was increased (Wilcoxon p-adjusted 1×10^{-8}), alongside with epicardial gene expression (not significant).

Additionally, we performed differential expression analysis on each of the KO conditions versus their *TRAC* controls (Table S3) and performed gene ontology term enrichment analysis on these gene sets (Table S3). The ventricular *ZNF711*-KO samples exhibited significant downregulation (p-adjusted < 0.05) of general (*TNNT2*, *NKX2-5*, *MYL7*, *CDH2*, and *TBX20*) and ventricular (*PLXNA4*, *IRX4*, *VCAM1*, *HEY2*, and *MYH7*) CM markers (Figures 5D and S8F and Table S3) and gene ontology terms (Table S3). This was not observed in the RA-treated atrial *ZNF711*-KO samples (Figure S8F and Table S3), in which upregulated genes were enriched for the terms *muscle cell differentiation* and *muscle system process* (Table S3). This suggests that the inhibition of CM differentiation observed in ventricular cultures was rescued by RA in the atrial *ZNF711*-KO cultures. To characterize this in more detail, *ZNF711*-KO up- and downregulated genes were used to calculate module scores in the single-cell *in vitro* atlas (Figure 5E). The ventricular *ZNF711*-KO downregulated targets (Figure 5E, left panel) show high expression in all of the CM-committed clusters within the atlas, whereas the ventricular *ZNF711*-KO upregulated genes are expressed in the non-CM branches of the roadmap (Figure 5E, middle-left). These results were corroborated by the increased NR2F2 protein levels measured in a NKX2-5-negative population (Figures S8C and S8D). Moreover, in these ventricular *ZNF711*-KO cultures, we found increased expression levels of *COL3A1*, known fetal epicardial markers (*SFRP2* and *TNNT1*) (Meier et al., 2023), and epicardial markers from our top 200 markers list (*COL9A3*, *KRT8*, *SFRP5*, *SULF1*, and *BCN2*; Table S3; all p-adjusted < 0.05). These data indicate a shift in populations from CMs to non-CMs. Conversely, the atrial *ZNF711*-KO downregulated genes were mostly expressed in the non-CM populations and CM progenitors (Figure 5E, middle-right), and upregulated genes showed specific expression in later CM differentiation stages of the roadmap (Figure 5E, right panel). These data show that *ZNF711*-KO hampered CM differentiation and increased both progenitor and non-CM signatures in the absence

(E) The *in vitro* atlas (Figure 1) labeled with compound gene expression levels (module scores) based on the gene groups from left to right: non-RA down- (log2FC < 0), non-RA up- (log2FC > 0), +RA down-, and +RA upregulated genes, based on significance (p-adjusted < 0.05) upon *ZNF711*-KO. CT, control; aCM, atrial; vCM, ventricular; RA, retinoic acid; DE, differentially expressed; log2FC, log2 (expression fold change between KO and CT).

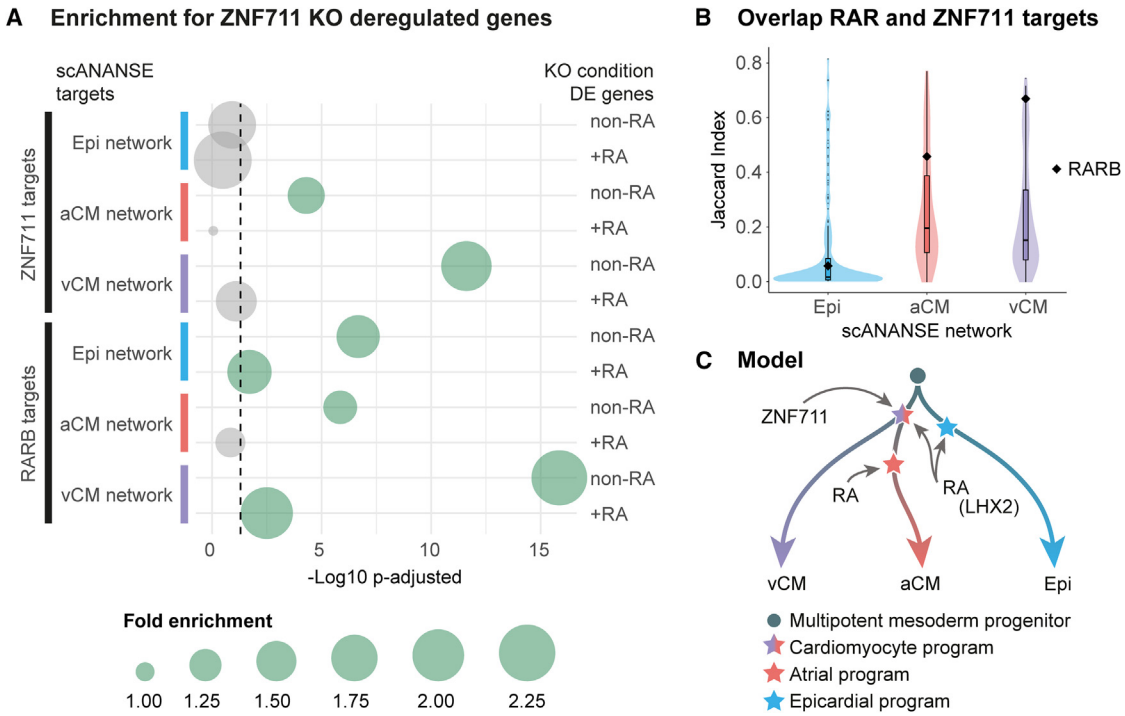

Figure 6. Enrichment for ZNF711 targets in the scANANSE networks and proposed model

(A) Enrichment of ANANSE-predicted network targets among differentially expressed genes in ZNF711-KO cardiac EBs. Bubble size represents fold enrichment, and the x axis shows multiple-testing corrected hypergeometric test *p* values. Indicated on the left is the regulator (ZNF711 and RARB) for which the predicted targets were selected from each of the cell type-specific scANANSE networks. On the right, conditions are indicated from which *ZNF711*-KO differential genes were selected, non-RA (ventricular) or +RA (atrial). The dashed line visualizes the *p*-adjusted value of 0.05. This figure represents a subset of all comparisons (cf. Figure S9 and Table S4 for all comparisons).

(B) Violin plots show overlap (Jaccard Index) between cell type-specific ANANSE-predicted targets of ZNF711 and RARB and other transcription factors (violin plots). The black diamonds indicate fold enrichment of overlap between ZNF711 and RARB targets for each of the networks. Full table is given in Table S4.

(C) Model of gene regulation (signified by the gray arrows) for balanced lineage commitment of progenitors to epicardial cells and atrial and ventricular CMs (thick colored arrows) by concerted action of *ZNF711*, *LHX2*, and RA. ZNF711 regulates important genes shared between the aCM and vCM lineage (purple-red star), which are dysregulated upon knockout of this factor. Treatment with RA rescues the effect of ZNF711 in the atrial conditions, explained by a significant overlap in target genes between the two (arrow of RA to purple-red star). Red star signifies the genes promoting aCM identity. RA also regulates genes that promote an epicardial fate (blue star). LHX2 appears to co-regulate both ZNF711 and RA-regulated genes (cf. Figure S9B) but does not act redundantly with RA. Rather, the defects in gene expression are mostly observed in presence of RA (Table S2).

of RA, whereas this effect was completely rescued by administration of RA.

The ventricular *ZNF503*-KO cultures showed a significant decrease in endothelial lineage markers, whereas the vCM markers were upregulated in ventricular cultures (Figure 5C). Differential expression testing in the *ZNF503*-KO EBs, however, only resulted in very few differentially expressed genes (DE genes) in either condition (Table S3). The *LHX2*-KO showed an increase in vCM and aCM markers (Wilcoxon *p*-adjusted 1.8×10^{-2} and 1.2×10^{-8}, respectively) in the ventricular EB cultures (Figure 5C and Table S3). In the atrial cultures, a significant decrease in fibroblast/smooth muscle markers (Wilcoxon *p*-adjusted 3.1×10^{-3}) and aCM progenitor markers (Wilcoxon *p*-adjusted 3.5×10^{-2}) was observed, to the benefit of the "other" cluster (Wilcoxon *p*-adjusted 3.4×10^{-4}).

Combined regulation of RARB and ZNF711

Given this dynamic re-routing of cardiac progenitors along different lineages, we wondered how the observed transcriptomic changes related to both the GRNs and the transcription factor motif content in our chromatin accessibility data. We therefore determined the overlap between *ZNF711*-KO DE genes and the ZNF711 targets predicted by scANANSE (Figures 6A and S9A and Table S3,

see methods). Since scANANSE generates cell type-specific GRNs, we performed this test for the vCM, aCM, and epicardial networks. The scANANSE ZNF711 targets were enriched for the ventricular *ZNF711*-KO DE genes, in both the vCM and aCM networks (fold enrichment 1.4 and 1.9, hypergeometric *p*-adjusted 5×10^{-5} and 2.4×10^{-12}, respectively), but not in the epicardial network, whereas no enrichment was found for the DE genes in the RA-treated (atrial) condition in any of the cell networks (Figure 6A). These findings confirm the predictive power of our scANANSE inferred networks. This also suggests that *ZNF711*-KO is directly required for the shared atrial-ventricular CM program but that RA rescues this program while also conferring an atrial identity to the resulting CMs.

Interestingly, performing the same test with the targets predicted by scANANSE for RARB showed significant enrichment of predicted RARB targets among the DE genes in the ventricular (non-RA) *ZNF711*-KO cultures (Figures 6A and S9A and Table S4). To establish how this overlap between RARB and ZNF711 targets compares to other regulators, we determined the relative overlap of targets between ZNF711 and all other transcription factors in the cell type networks (methods, Table S4), using the Jaccard index (shared targets divided by all targets of the two transcription factors), and compared the distribution of Jaccard indices with the index of the ZNF711-RARB pair (Figure 6B). The networks are highly interconnected (cf. Figures 4E and 4F), and many show extensive overlap in targets (Figure 6B). ZNF711 showed a large overlap with RARB targets compared to other regulators in this network, especially within the vCM network (Jaccard index 0.67, 26-fold-enrichment, hypergeometric *p*-adjusted < 1e−100). In the aCM network, these shared targets were also enriched, although to a lesser degree (Jaccard index 0.46, 8.8-fold, hypergeometric *p*-adjusted < 1e−100). These shared targets can explain how RA treatment can rescue CM differentiation in *ZNF711*-KO atrial EB cultures.

These analyses also showed significantly enriched overlaps of LHX2 targets in the epicardial and CM networks and *LHX2*-KO DE genes, in addition to evidence for shared targets between LHX2, ZNF711, and RARB but only under RA-treatment conditions in the epicardial and aCM networks (Figure S9 and Table S4).

As summarized in our model (Figure 6C), the data uncover how the balance of lineage decisions of cardiac progenitors is shifted by genetic perturbations and is modified by RA, a natural cardiac crescent morphogen. We find that *ZNF711* is important for a general CM program including the expression of structural sarcomere genes, but only in the absence of RA. The resulting block in CM differentiation redirects progenitors toward the epicardial and endodermal lineages. RA rescues the defect on the general CM program in the absence of ZNF711 and induces the aCM identity. LHX2 appears to co-regulate many of the RA targets to promote epicardial and CM gene expression.

DISCUSSION

We present a roadmap of human cardiac differentiation, detailing the steps of lineage commitment in cardiac monolayer, EB, and EHT cultures. We identified similar multilineage compositions within the atrial and ventricular EB cultures as reported in other cardiac organoid protocols (Meier et al., 2023; Silva et al., 2021). In our experiments, the EBs showcased a plasticity of multipotent progenitor cells that was susceptible to patterning by RA. Because of this high level of plasticity and the ability to culture CMs of various subtypes (Schwach et al., 2017; Zawada et al., 2023), detailed deconstruction of the developmental steps within the culture is necessary to understand and optimize the cell type composition. The specification of pSHF progenitors directed CMs toward an atrial identity, as expected; however, other cell lineages (endothelial, epicardial, fibroblast, and smooth muscle cell-like cells) were minimally affected. Our analysis not only identified known and candidate regulators but also helped interpreting the results from KO studies. This revealed that *ZNF711* plays a critical role in safeguarding the general CM program, whereas, in the absence of both *ZNF711* and RA, a major shift toward the non-CM gene expression programs is observed.

Epicardial and anterior endoderm cell populations have been observed in previous studies (Drakhlis et al., 2021; Hofbauer et al., 2021; Meier et al., 2023; Silva et al., 2021; Zawada et al., 2023). Our findings corroborate these observations and demonstrate that these populations can emerge independently of RA treatment (Drakhlis et al., 2021; Silva et al., 2021). This was confirmed by the expression of markers of the juxta-cardiac field and pre-epicardial cells (Meier et al., 2023; Zawada et al., 2023). Paracrine signaling from endodermal and epicardial populations has been reported to be beneficial for both the epicardial and CM cell populations (Quijada et al., 2020). Moreover, anterior endoderm is essential for vertebrate heart development and morphogenesis (Nascone and Mercola, 1995; Withington et al., 2001).

In our pursuit of candidate regulators, we identified an important role for *ZNF711*, a gene about which comparatively little is known. Mutations in *ZNF711* have been associated with X-linked intellectual disability and an altered DNA methylation signature in blood (Wang et al., 2022). *ZNF711* is a member of a small family of zinc-finger genes that encode a similar N-terminal acidic activation domain (Mardon et al., 1990; Ni et al., 2020). Moreover, ZNF711

can bind CpG island promoters where it can recruit PHF8, a histone H3K9 demethylase (Kleine-Kohlbrecher et al., 2010). Notably, *ZNF711* orthologs are found in the genomes of jawed vertebrates but not in those of invertebrate animals. Although shared among most bilaterian animals, the heart has evolved significantly in vertebrates, including the addition of chambers and the endocardial and epicardial layers (Carmona et al., 2010; Simões-Costa et al., 2005). The RA pathway was co-opted to derive aCMs and the epicardial lineage from mesodermal precursors. This may have required changes to safeguard the FHF-aSHF-derived vCM program. Our research reveals that *ZNF711* is important for CM differentiation in the absence of RA. In scenarios where both ZNF711 and RA are absent, there is a shift toward the differentiation of epicardial and other lineages at the expense of ventricular CMs. CM commitment is rescued by RA, while simultaneously endowing the CMs with a posteriorized atrial gene expression identity. Consistent with this rescue, we find that regulatory elements of the genes involved contain motifs for both ZNF711 and RA receptors, providing a mechanism for balanced lineage commitment both in the absence and the presence of RA. Given the plasticity of cardiac mesoderm and heart field progenitors, which are readily redirected to different cell lineages, safeguards are necessary for such a balanced lineage differentiation, and ZNF711 appears to have an important role in securing the CM program.

The cardiac organoid models and CM differentiation protocols available to date have been obtained by extensive experimentation and diligent optimization. These models contain different cell types and cell states, reflecting both lineage potential and culture conditions. Further effort will be required to improve these human stem cell-based models by leveraging single-cell roadmaps and GRNs. This will increase our fundamental understanding of the heart as a complex tissue, while providing a major impetus for analyses of heart disease mechanisms, heart regeneration, and drug screening.

METHODS

Detailed methods can be found in the supplemental information and are described in brief in the following.

Culture, differentiation, and imaging of vCMs and aCMs

The hESC line NKX2.5$^{EGFP/+}$COUP-TFII$^{mCherry/+}$ (Schwach et al., 2017) was used throughout this study. Differentiation toward ventricular monolayers (vCM-Mon) (Birket et al., 2015) and atrial or ventricular EBs (aCM- or vCM-EBs) (Schwach et al., 2022) has been described. See supplemental information for cell line maintenance and characterization, culture details, and the procedures using antibodies and dyes for immunohistochemistry and confocal and optical membrane potential imaging.

Generation of EHTs

EHTs from sorted vCM-mon (NKX2.5$^{EGFP/+}$ positive and COUP-TFII$^{mCherry/+}$ negative) and aCM-EBs (NKX2.5$^{EGFP/+}$ positive and COUP-TFII$^{mCherry/+}$ positive) were mixed, respectively, in a ratio of 80:20 with sorted non-CM (NKX2.5$^{EGFP/+}$ negative). EHTs were formed by following the protocol as described (Ribeiro et al., 2022).

FACS sorting and single-cell genomic library preparations

Time points harvested for the single-cell atlas were fluorescence-activated cell sorting (FACS) sorted into 384-well plates, and a total of 63 single-cell RNA sequencing (scRNA-seq) libraries were generated with the plate-based CEL-Seq2 protocol (Hashimshony et al., 2016). A detailed description of the batches and steps of library generation is provided in Table S5 and supplemental information. The 10× Multiome protocol was used to sample day 8 atrial and ventricular EB cultures.

Generation and validation of LHX2, ZNF711, and ZNF503 CRISPR-Cas9 KOs

KOs were performed in the hESC line NKX2.5$^{EGFP/+}$COUP-TFII$^{mCherry/+}$. The KO cultures were harvested at day 14 for flow cytometry and bulk RNA-seq.

Genome mapping of NGS data

All new produced next-generation sequencing (NGS) data in this manuscript were mapped against the GRCh38 genome. The scRNA-seq data and bulk RNA-seq data were mapped using Seq2Science v.0.9.6 (van der Sande et al., 2023). Data of the 10 × Multiome was mapped using the 10 × Genomics Cell Ranger ARC software.

Constructing the single-cell datasets and validation

The scRNA-seq libraries from the different time points, methods, and lineages from multiple experiments (Table S5) were integrated using the canonical correlation analysis (CCA) implementation of Seurat in R (Hao et al., 2021). By comparing the anchors found between the separate differentiation experiments, this data integration process was validated. *In vivo* human fetal data were processed after mapping by the authors (Asp et al., 2019; Cui et al., 2019) and were used to annotate the single-cell roadmap, by using the *TransferData* functionality in Seurat. RNA velocity analysis was performed in Python, using scVelo (Bergen et al., 2020). More details on these analytical steps, as well as the differential gene testing

used on EB time points and RA-related gene sets, are provided in the supplemental information.

Multiome data analyses and bulk RNA-seq analyses

The multiome samples were also integrated using Seurat, and the single-cell transcriptomes of the clusters were compared with the plate-based scRNA-seq atlas clusters by means of Pearson correlation. The scATAC-seq modality was processed using Signac and used in pseudobulk to run scANANSE per cluster (Smits et al., 2023). To visualize the GRNs shown in this manuscript, only interactions with a score >0.8 were selected. The processing and differential expression testing performed on the RNA-seq data of the KOs were performed with DESeq2 (Love et al., 2014).

RESOURCE AVAILABILITY

Lead contact

Requests for further information and resources should be directed to the lead contact, Gert Jan C. Veenstra (gertjan.veenstra@ru.nl).

Materials availability

This study did not generate new unique reagents.

Data and code availability

All NGS data are available on GEO with the temporal scRNA-seq data at GSE263193, the multiome day 8 EB samples at GSE263326, and the RNA-seq data of the KO samples at GSE263325. Published data were obtained from GSE106118 (Cui et al., 2019) or as filtered matrices published on the author's website (Asp, 2021; Asp et al., 2019). The single-cell temporal roadmap object for visualization can be downloaded through Zenodo via https://doi.org/10.5281/zenodo.10932845. The per-cluster pseudobulk scATAC-seq profiles can be viewed in the Genome Browser at https://genome.ucsc.edu/s/rebecza/scRoadmap_CardiacDiffs_hg38. All used software is mentioned in the methods; the custom R and Python scripts used for the analyses, as well as instructions on how to visualize the single-cell roadmap data in an interactive user interface, are available on GitHub at https://github.com/Rebecza/scRoadmap_CardiacDiffs.

ACKNOWLEDGMENTS

This work was funded by a ZonMw TOP grant (project number 91217061) to R.P. and G.J.C.V.

AUTHOR CONTRIBUTIONS

R.R.S. conceived experiments, generated libraries for all next-generation sequencing (NGS) methods used in the manuscript, led the computational analysis, and wrote the manuscript. C.C.-F. conceived experiments, performed all cell culture work used in the manuscript, harvested and sorted the cells, generated the CRISPR-Cas9 knockout lines, and wrote the manuscript. M.B. generated bulk RNA sequencing libraries and performed the sequencing for all NGS libraries used in the manuscript. V.S. conceived experiments. R.P. conceived experiments, supervised the experiments involving stem cell differentiation, wrote the manuscript, and generated funding for the work. G.J.C.V. conceived experiments, supervised computational genomics analysis, wrote the manuscript, and generated funding for the work.

DECLARATION OF INTERESTS

R.P. is a cofounder of Pluriomics (Ncardia) and River BioMedics BV.

SUPPLEMENTAL INFORMATION

Supplemental information can be found online at https://doi.org/10.1016/j.stemcr.2025.102422.

Received: November 6, 2024
Revised: January 27, 2025
Accepted: January 28, 2025
Published: February 27, 2025

REFERENCES

Ameen, M., Sundaram, L., Shen, M., Banerjee, A., Kundu, S., Nair, S., Shcherbina, A., Gu, M., Wilson, K.D., Varadarajan, A., et al. (2022). Integrative single-cell analysis of cardiogenesis identifies developmental trajectories and non-coding mutations in congenital heart disease. Cell *185*, 4937–4953.e23. https://doi.org/10.1016/J.CELL.2022.11.028.

Ang, L.T., Tan, A.K.Y., Autio, M.I., Goh, S.H., Choo, S.H., Lee, K.L., Tan, J., Pan, B., Lee, J.J.H., Lum, J.J., et al. (2018). A Roadmap for Human Liver Differentiation from Pluripotent Stem Cells. Cell Rep. *22*, 2190–2205. https://doi.org/10.1016/j.celrep.2018.01.087.

Asp, M. (2021). Developmental heart - filtered and unfiltered count matrices and meta tables. Mendeley Data Version *2*. https://doi.org/10.17632/MBVHHF8M62.2.

Asp, M., Giacomello, S., Larsson, L., Wu, C., Fürth, D., Qian, X., Wärdell, E., Custodio, J., Reimegård, J., Salmén, F., et al. (2019). A Spatiotemporal Organ-Wide Gene Expression and Cell Atlas of the Developing Human Heart. Cell *179*, 1647–1660.e19. https://doi.org/10.1016/j.cell.2019.11.025.

Bergen, V., Lange, M., Peidli, S., Wolf, F.A., and Theis, F.J. (2020). Generalizing RNA velocity to transient cell states through dynamical modeling. Nat. Biotechnol. *38*, 1408–1414. https://doi.org/10.1038/s41587-020-0591-3.

Birket, M.J., Ribeiro, M.C., Kosmidis, G., Ward, D., Leitoguinho, A.R., van de Pol, V., Dambrot, C., Devalla, H.D., Davis, R.P., Mastroberardino, P.G., et al. (2015). Contractile Defect Caused by Mutation in MYBPC3 Revealed under Conditions Optimized for Human PSC-Cardiomyocyte Function. Cell Rep. *13*, 733–745. https://doi.org/10.1016/j.celrep.2015.09.025.

Boobalan, E., Thompson, A.H., Alur, R.P., McGaughey, D.M., Dong, L., Shih, G., Vieta-Ferrer, E.R., Onojafe, I.F., Kalaskar, V.K., Arno, G., et al. (2022). Zfp503/Nlz2 Is Required for RPE Differentiation and Optic Fissure Closure. Investig. Ophthalmol. Vis. Sci. *63*, 5. https://doi.org/10.1167/IOVS.63.12.5.

Branco, M.A., Dias, T.P., Cabral, J.M.S., Pinto-do-Ó, P., and Diogo, M.M. (2022). Human multilineage pro-epicardium/foregut organoids support the development of an epicardium/myocardium

organoid. Nat. Commun. *13*, 6981. https://doi.org/10.1038/s41467-022-34730-7.

Buckingham, M., Meilhac, S., and Zaffran, S. (2005). Building the mammalian heart from two sources of myocardial cells. Nat. Rev. Genet. *6*, 826–835. https://doi.org/10.1038/nrg1710.

Carmona, R., Guadix, J.A., Cano, E., Ruiz-Villalba, A., Portillo-Sánchez, V., Pérez-Pomares, J.M., and Muñoz-Chápuli, R. (2010). The embryonic epicardium: an essential element of cardiac development. J. Cell Mol. Med. *14*, 2066–2072. https://doi.org/10.1111/J.1582-4934.2010.01088.X.

Churko, J.M., Garg, P., Treutlein, B., Venkatasubramanian, M., Wu, H., Lee, J., Wessells, Q.N., Chen, S.Y., Chen, W.Y., Chetal, K., et al. (2018). Defining human cardiac transcription factor hierarchies using integrated single-cell heterogeneity analysis. Nat. Commun. *9*, 4906. https://doi.org/10.1038/s41467-018-07333-4.

Cui, Y., Zheng, Y., Liu, X., Yan, L., Fan, X., Yong, J., Hu, Y., Dong, J., Li, Q., Wu, X., et al. (2019). Single-Cell Transcriptome Analysis Maps the Developmental Track of the Human Heart. Cell Rep. *26*, 1934–1950.e5. https://doi.org/10.1016/j.celrep.2019.01.079.

Devalla, H.D., and Passier, R. (2018). Cardiac differentiation of pluripotent stem cells and implications for modeling the heart in health and disease. Sci. Transl. Med. *10*, eaah5457. https://doi.org/10.1126/scitranslmed.aah5457.

Devalla, H.D., Schwach, V., Ford, J.W., Milnes, J.T., El-Haou, S., Jackson, C., Gkatzis, K., Elliott, D.A., Chuva de Sousa Lopes, S.M., Mummery, C.L., et al. (2015). Atrial-like cardiomyocytes from human pluripotent stem cells are a robust preclinical model for assessing atrial-selective pharmacology. EMBO Mol. Med. *7*, 394–410.

Drakhlis, L., Biswanath, S., Farr, C.-M., Lupanow, V., Teske, J., Ritzenhoff, K., Franke, A., Manstein, F., Bolesani, E., Kempf, H., et al. (2021). Human heart-forming organoids recapitulate early heart and foregut development. Nat. Biotechnol. *39*, 737–746. https://doi.org/10.1038/s41587-021-00815-9.

Farah, E.N., Hu, R.K., Kern, C., Zhang, Q., Lu, T.Y., Ma, Q., Tran, S., Zhang, B., Carlin, D., Monell, A., et al. (2024). Spatially organized cellular communities form the developing human heart. Nature *627*, 854–864. https://doi.org/10.1038/S41586-024-07171-Z.

Grancharova, T., Gerbin, K.A., Rosenberg, A.B., Roco, C.M., Arakaki, J.E., DeLizo, C.M., Dinh, S.Q., Donovan-Maiye, R.M., Hirano, M., Nelson, A.M., et al. (2021). A comprehensive analysis of gene expression changes in a high replicate and open-source dataset of differentiating hiPSC-derived cardiomyocytes. Sci. Rep. *11*, 15845. https://doi.org/10.1038/s41598-021-94732-1.

Guo, Y., and Pu, W.T. (2020). Cardiomyocyte maturation: New phase in development. Circ. Res. *126*, 1086–1106. https://doi.org/10.1161/CIRCRESAHA.119.315862.

Hanawa, M., Takayama, K., Sakurai, F., Tachibana, M., and Mizuguchi, H. (2017). Hepatocyte Nuclear Factor 4 Alpha Promotes Definitive Endoderm Differentiation from Human Induced Pluripotent Stem Cells. Stem Cell Rev. Rep. *13*, 542–551. https://doi.org/10.1007/S12015-016-9709-X.

Hao, Y., Hao, S., Andersen-Nissen, E., Mauck, W.M., Zheng, S., Butler, A., Lee, M.J., Wilk, A.J., Darby, C., Zager, M., et al. (2021). Integrated analysis of multimodal single-cell data. Cell *184*, 3573–3587.e29. https://doi.org/10.1016/J.CELL.2021.04.048.

Harlaar, N., Dekker, S.O., Zhang, J., Snabel, R.R., Veldkamp, M.W., Verkerk, A.O., Fabres, C.C., Schwach, V., Lerink, L.J.S., Rivaud, M.R., et al. (2022). Conditional immortalization of human atrial myocytes for the generation of *in vitro* models of atrial fibrillation. Nat. Biomed. Eng. *6*, 389–402. https://doi.org/10.1038/s41551-021-00827-5.

Hashimshony, T., Senderovich, N., Avital, G., Klochendler, A., de Leeuw, Y., Anavy, L., Gennert, D., Li, S., Livak, K.J., Rozenblatt-Rosen, O., et al. (2016). CEL-Seq2: Sensitive highly-multiplexed single-cell RNA-Seq. Genome Biol. *17*, 77. https://doi.org/10.1186/s13059-016-0938-8.

Hofbauer, P., Jahnel, S.M., Papai, N., Giesshammer, M., Deyett, A., Schmidt, C., Penc, M., Tavernini, K., Grdseloff, N., Meledeth, C., et al. (2021). Cardioids reveal self-organizing principles of human cardiogenesis. Cell *184*, 3299–3317.e22. https://doi.org/10.1016/J.CELL.2021.04.034.

Itoh, N., Ohta, H., Nakayama, Y., and Konishi, M. (2016). Roles of FGF Signals in Heart Development, Health, and Disease. Front. Cell Dev. Biol. *4*, 110. https://doi.org/10.3389/FCELL.2016.00110.

Kanai-Azuma, M., Kanai, Y., Gad, J.M., Tajima, Y., Taya, C., Kurohmaru, M., Sanai, Y., Yonekawa, H., Yazaki, K., Tam, P.P.L., and Hayashi, Y. (2002). Depletion of definitive gut endoderm in Sox17-null mutant mice. Development *129*, 2367–2379. https://doi.org/10.1242/DEV.129.10.2367.

Kanki, Y., Kohro, T., Jiang, S., Tsutsumi, S., Mimura, I., Suehiro, J.I., Wada, Y., Ohta, Y., Ihara, S., Iwanari, H., et al. (2011). Epigenetically coordinated GATA2 binding is necessary for endothelium-specific endomucin expression. EMBO J. *30*, 2582–2595. https://doi.org/10.1038/EMBOJ.2011.173.

Kannan, S., Farid, M., Lin, B.L., Miyamoto, M., and Kwon, C. (2021). Transcriptomic entropy benchmarks stem cell-derived cardiomyocyte maturation against endogenous tissue at single cell level. PLoS Comput. Biol. *17*, e1009305. https://doi.org/10.1371/JOURNAL.PCBI.1009305.

Kim, K.H., Rosen, A., Hussein, S.M.I., Puviindran, V., Korogyi, A.S., Chiarello, C., Nagy, A., Hui, C.C., and Backx, P.H. (2016). Irx3 is required for postnatal maturation of the mouse ventricular conduction system. Sci. Rep. *6*, 19197. https://doi.org/10.1038/srep19197.

Kleine-Kohlbrecher, D., Christensen, J., Vandamme, J., Abarrategui, I., Bak, M., Tommerup, N., Shi, X., Gozani, O., Rappsilber, J., Salcini, A.E., and Helin, K. (2010). A Functional Link between the Histone Demethylase PHF8 and the Transcription Factor ZNF711 in X-Linked Mental Retardation. Mol. Cell *38*, 165–178. https://doi.org/10.1016/J.MOLCEL.2010.03.002.

Lescroart, F., and Zaffran, S. (2018). Hox and Tale transcription factors in heart development and disease. Int. J. Dev. Biol. *62*, 837–846. https://doi.org/10.1387/ijdb.180192sz.

Lescroart, F., and Zaffran, S. (2022). Single Cell Approaches to Understand the Earliest Steps in Heart Development. Curr. Cardiol. Rep. *24*, 611–621. https://doi.org/10.1007/S11886-022-01681-W.

Lescroart, F., Chabab, S., Lin, X., Rulands, S., Paulissen, C., Rodolosse, A., Auer, H., Achouri, Y., Dubois, C., Bondue, A., et al.

(2014). Early lineage restriction in temporally distinct populations of Mesp1 progenitors during mammalian heart development. Nat. Cell Biol. *16*, 829–840. https://doi.org/10.1038/ncb3024.

Love, M.I., Huber, W., and Anders, S. (2014). Moderated estimation of fold change and dispersion for RNA-seq data with DESeq2. Genome Biol. *15*, 550. https://doi.org/10.1186/S13059-014-0550-8.

Mardon, G., Luoh, S.-W., Simpson, E.M., Gill, G., Brown, L.G., and Page, D.C. (1990). Mouse Zfx protein is similar to Zfy-2: each contains an acidic activating domain and 13 zinc fingers. Mol. Cell Biol. *10*, 681–688. https://doi.org/10.1128/MCB.10.2.681-688.1990.

Meier, A.B., Zawada, D., De Angelis, M.T., Martens, L.D., Santamaria, G., Zengerle, S., Nowak-Imialek, M., Kornherr, J., Zhang, F., Tian, Q., et al. (2023). Epicardioid single-cell genomics uncovers principles of human epicardium biology in heart development and disease. Nat. Biotechnol. *41*, 1787–1800. https://doi.org/10.1038/s41587-023-01718-7.

Meilhac, S.M., and Buckingham, M.E. (2018). The deployment of cell lineages that form the mammalian heart. Nat. Rev. Cardiol. *15*, 705–724. https://doi.org/10.1038/s41569-018-0086-9.

Mononen, M.M., Leung, C.Y., Xu, J., Chien, K.R., and Kenneth Chien, C.R. (2020). Trajectory mapping of human embryonic stem cell cardiogenesis reveals lineage branch points and an ISL1 progenitor-derived cardiac fibroblast lineage. Stem Cell. *38*, 1267–1278. https://doi.org/10.1002/stem.3236.

Nakamura, M., Choe, S.K., Runko, A.P., Gardner, P.D., and Sagerström, C.G. (2008). Nlz1/Znf703 acts as a repressor of transcription. BMC Dev. Biol. *8*, 108. https://doi.org/10.1186/1471-213X-8-108.

Nascone, N., and Mercola, M. (1995). An inductive role for the endoderm in Xenopus cardiogenesis. Development *121*, 515–523. https://doi.org/10.1242/DEV.121.2.515.

Ni, W., Perez, A.A., Schreiner, S., Nicolet, C.M., and Farnham, P.J. (2020). Characterization of the ZFX family of transcription factors that bind downstream of the start site of CpG island promoters. Nucleic Acids Res. *48*, 5986–6000. https://doi.org/10.1093/NAR/GKAA384.

Pezhouman, A., Nguyen, N.B., Sercel, A.J., Nguyen, T.L., Daraei, A., Sabri, S., Chapski, D.J., Zheng, M., Patananan, A.N., Ernst, J., et al. (2021). Transcriptional, Electrophysiological, and Metabolic Characterizations of hESC-Derived First and Second Heart Fields Demonstrate a Potential Role of TBX5 in Cardiomyocyte Maturation. Front. Cell Dev. Biol. *9*, 787684. https://doi.org/10.3389/FCELL.2021.787684.

Protze, S.I., Lee, J.H., and Keller, G.M. (2019). Human Pluripotent Stem Cell-Derived Cardiovascular Cells: From Developmental Biology to Therapeutic Applications. Cell Stem Cell *25*, 311–327. https://doi.org/10.1016/J.STEM.2019.07.010.

Quaranta, R., Fell, J., Rühle, F., Rao, J., Piccini, I., Araúzo-Bravo, M.J., Verkerk, A.O., Stoll, M., and Greber, B. (2018). Revised roles of ISL1 in a hES cell-based model of human heart chamber specification. Elife *7*, e31706. https://doi.org/10.7554/ELIFE.31706.

Quijada, P., Trembley, M.A., and Small, E.M. (2020). The Role of the Epicardium during Heart Development and Repair. Circ. Res. *126*, 377–394. https://doi.org/10.1161/CIRCRESAHA.119.315857.

Rana, M.S., Théveniau-Ruissy, M., De Bono, C., Mesbah, K., Francou, A., Rammah, M., Domínguez, J.N., Roux, M., Laforest, B., Anderson, R.H., et al. (2014). Tbx1 coordinates addition of posterior second heart field progenitor cells to the arterial and venous poles of the heart. Circ. Res. *115*, 790–799. https://doi.org/10.1161/CIRCRESAHA.115.305020.

Ribeiro, M.C., Rivera-Arbeláez, J.M., Cofiño-Fabres, C., Schwach, V., Slaats, R.H., Ten Den, S.A., Vermeul, K., van den Berg, A., Pérez-Pomares, J.M., Segerink, L.I., et al. (2022). A New Versatile Platform for Assessment of Improved Cardiac Performance in Human-Engineered Heart Tissues. J. Personalized Med. *12*, 12. https://doi.org/10.3390/JPM12020214/S1.

Roux, M., Zaffran, S., Zappavigna, V., and Conway, S.J. (2016). Hox Genes in Cardiovascular Development and Diseases. J. Dev. Biol. *4*, 14. https://doi.org/10.3390/JDB4020014.

Sahara, M., Santoro, F., Sohlmér, J., Zhou, C., Witman, N., Leung, C.Y., Mononen, M., Bylund, K., Gruber, P., and Chien, K.R. (2019). Population and Single-Cell Analysis of Human Cardiogenesis Reveals Unique LGR5 Ventricular Progenitors in Embryonic Outflow Tract. Dev. Cell *48*, 475–490.e7. https://doi.org/10.1016/j.devcel.2019.01.005.

van der Sande, M., Frölich, S., Schäfers, T., Smits, J.G.A., Snabel, R.R., Rinzema, S., and van Heeringen, S.J. (2023). Seq2science: an end-to-end workflow for functional genomics analysis. PeerJ *11*, e16380. https://doi.org/10.7717/PEERJ.16380.

Scheibner, K., Schirge, S., Burtscher, I., Büttner, M., Sterr, M., Yang, D., Böttcher, A., Ansarullah, Irmler, M., Beckers, J., et al. (2021). Epithelial cell plasticity drives endoderm formation during gastrulation. Nat. Cell Biol. *23*, 692–703. https://doi.org/10.1038/S41556-021-00694-X.

Schwach, V., Verkerk, A.O., Mol, M., Monshouwer-Kloots, J.J., Devalla, H.D., Orlova, V.V., Anastassiadis, K., Mummery, C.L., Davis, R.P., and Passier, R. (2017). A COUP-TFII Human Embryonic Stem Cell Reporter Line to Identify and Select Atrial Cardiomyocytes. Stem Cell Rep. *9*, 1765–1779. https://doi.org/10.1016/j.stemcr.2017.10.024.

Schwach, V., Cofiño-Fabres, C., Ten Den, S.A., and Passier, R. (2022). Improved Atrial Differentiation of Human Pluripotent Stem Cells by Activation of Retinoic Acid Receptor Alpha (RARα). J. Personalized Med. *12*, 628. https://doi.org/10.3390/JPM12040628.

Shahi, P., Wang, C.Y., Lawson, D.A., Slorach, E.M., Lu, A., Yu, Y., Lai, M.D., Gonzalez Velozo, H., and Werb, Z. (2017). ZNF503/Zpo2 drives aggressive breast cancer progression by down-regulation of GATA3 expression. Proc. Natl. Acad. Sci. USA *114*, 3169–3174. https://doi.org/10.1073/PNAS.1701690114.

Silva, A.C., Matthys, O.B., Joy, D.A., Kauss, M.A., Natarajan, V., Lai, M.H., Turaga, D., Blair, A.P., Alexanian, M., Bruneau, B.G., and McDevitt, T.C. (2021). Co-emergence of cardiac and gut tissues promotes cardiomyocyte maturation within human iPSC-derived organoids. Stem Cell. *28*, 2137–2152.e6. https://doi.org/10.1016/j.stem.2021.11.007.

Simões-Costa, M.S., Vasconcelos, M., Sampaio, A.C., Cravo, R.M., Linhares, V.L., Hochgreb, T., Yan, C.Y.I., Davidson, B., and Xavier-Neto, J. (2005). The evolutionary origin of cardiac chambers. Dev. Biol. *277*, 1–15. https://doi.org/10.1016/J.YDBIO.2004.09.026.

Smits, J.G.A., Arts, J.A., Frölich, S., Snabel, R.R., Heuts, B.M.H., Martens, J.H.A., van Heeringen, S.J., and Zhou, H. (2023). scANANSE gene regulatory network and motif analysis of single-cell clusters. F1000Research *12*, 243. https://doi.org/10.12688/f1000research.130530.1.

Steimle, J.D., and Moskowitz, I.P. (2017). TBX5: A Key Regulator of Heart Development. Curr. Top. Dev. Biol. *122*, 195–221. https://doi.org/10.1016/bs.ctdb.2016.08.008.

Sweat, M.E., Cao, Y., Zhang, X., Burnicka-Turek, O., Perez-Cervantes, C., Arulsamy, K., Lu, F., Keating, E.M., Akerberg, B.N., Ma, Q., et al. (2023). Tbx5 maintains atrial identity in post-natal cardiomyocytes by regulating an atrial-specific enhancer network. Nat. Cardiovasc. Res. *2*, 881–898. https://doi.org/10.1038/S44161-023-00334-7.

Takahashi, K., Tanabe, K., Ohnuki, M., Narita, M., Ichisaka, T., Tomoda, K., and Yamanaka, S. (2007). Induction of Pluripotent Stem Cells from Adult Human Fibroblasts by Defined Factors. Cell *131*, 861–872. https://doi.org/10.1016/j.cell.2007.11.019.

Thomson, J.A., Itskovitz-Eldor, J., Shapiro, S.S., Waknitz, M.A., Swiergiel, J.J., Marshall, V.S., and Jones, J.M. (1998). Embryonic stem cell lines derived from human blastocysts. Science *282*, 1145–1147. https://doi.org/10.1126/SCIENCE.282.5391.1145.

Tyser, R.C.V., Mahammadov, E., Nakanoh, S., Vallier, L., Scialdone, A., and Srinivas, S. (2021). Single-cell transcriptomic characterization of a gastrulating human embryo. Nature *600*, 285–289. https://doi.org/10.1038/s41586-021-04158-y.

Wang, J., Foroutan, A., Richardson, E., Skinner, S.A., Reilly, J., Kerkhof, J., Curry, C.J., Tarpey, P.S., Robertson, S.P., Maystadt, I., et al. (2022). Clinical findings and a DNA methylation signature in kindreds with alterations in ZNF711. Eur. J. Hum. Genet. *30*, 420–427. https://doi.org/10.1038/S41431-021-01018-1.

Wiesinger, A., Li, J., Fokkert, L., Bakker, P., Verkerk, A.O., Christoffels, V.M., Boink, G.J.J., and Devalla, H.D. (2022). A single cell transcriptional roadmap of human pacemaker cell differentiation. Elife *11*, e76781. https://doi.org/10.7554/ELIFE.76781.

Withington, S., Beddington, R., and Cooke, J. (2001). Foregut endoderm is required at head process stages for anteriormost neural patterning in chick. Development *128*, 309–320. https://doi.org/10.1242/DEV.128.3.309.

Xin, M., Davis, C.A., Molkentin, J.D., Lien, C.L., Duncan, S.A., Richardson, J.A., and Olson, E.N. (2006). A threshold of GATA4 and GATA6 expression is required for cardiovascular development. Proc. Natl. Acad. Sci. USA *103*, 11189–11194. https://doi.org/10.1073/PNAS.0604604103.

Yang, D., Gomez-Garcia, J., Funakoshi, S., Tran, T., Fernandes, I., Bader, G.D., Laflamme, M.A., and Keller, G.M. (2022). Modeling human multi-lineage heart field development with pluripotent stem cells. Cell Stem Cell *29*, 1382–1401.e8. https://doi.org/10.1016/J.STEM.2022.08.007.

Yu, J., Vodyanik, M.A., Smuga-Otto, K., Antosiewicz-Bourget, J., Frane, J.L., Tian, S., Nie, J., Jonsdottir, G.A., Ruotti, V., Stewart, R., et al. (2007). Induced pluripotent stem cell lines derived from human somatic cells. Science *318*, 1917–1920. https://doi.org/10.1126/SCIENCE.1151526.

Zawada, D., Kornherr, J., Meier, A.B., Santamaria, G., Dorn, T., Nowak-Imialek, M., Ortmann, D., Zhang, F., Lachmann, M., Dreßen, M., et al. (2023). Retinoic acid signaling modulation guides *in vitro* specification of human heart field-specific progenitor pools. Nat. Commun. *14*, 1722. https://doi.org/10.1038/s41467-023-36764-x.

Zeng, B., Liu, Z., Lu, Y., Zhong, S., Qin, S., Huang, L., Zeng, Y., Li, Z., Dong, H., Shi, Y., et al. (2023). The single-cell and spatial transcriptional landscape of human gastrulation and early brain development. Cell Stem Cell *30*, 851–866.e7. https://doi.org/10.1016/J.STEM.2023.04.016.

Zhang, Q., Jiang, J., Han, P., Yuan, Q., Zhang, J., Zhang, X., Xu, Y., Cao, H., Meng, Q., Chen, L., et al. (2011). Direct differentiation of atrial and ventricular myocytes from human embryonic stem cells by alternating retinoid signals. Cell Res. *21*, 579–587. https://doi.org/10.1038/cr.2010.163.